Supplementary Information

An atomistic model of solute transport across the blood-brain barrier

Christian Jorgensen,[1,4] Martin B. Ulmschneider,[2] Peter C. Searson[1,3,*]

[1]Institute for Nanobiotechnology, Johns Hopkins University, Baltimore, Maryland, USA
[2]Department of Chemistry, King's College, London, UK
[3]Department of Materials Science and Engineering, Johns Hopkins University, Baltimore, Maryland, USA

Contents:

[4] Current address: Department of Physics, Georgetown University, Washington DC, USA

Supplementary Information Text

Background

MD simulations are increasingly used in drug discovery and to study transport across various biological barriers[1-10] and the study of ligand-drug binding.[11-14] For example, multi-microsecond unbiased molecular dynamics (MD) simulations have been used to model cell membranes,[9] biased MD simulations have been used to model transport across (non-BBB) membranes,[3-5, 7] and unbiased MD simulations have been used to model transport across implicit (non-atomistic) membrane systems.[8] While there have been many analytical models of passive transport into the brain,[15-18] as well as MD simulations of simplified membrane systems,[19] there have been no atomistic simulations of a realistic model of the BBB.

Materials and Methods (Extended)

An atomic detail model of the BBB bilayer

An atomic detail molecular model of the apical hBMEC lipid bilayer was constructed by closely replicating physiological lipid compositions (**Figure 1A-B**).[20] The BBB bilayer model (96 lipids, area 25 nm^2) was set up using standard compositions for polarized endothelial cell membranes,[21-24] and consists of nine lipid types. The specific composition was: N-oleoyl-sphingomyelin (OSM; 18), 1-palmitoyl-2-oleoyl-glycero-3-phosphocholine (POPC; 4), 1-stearoyl-2-arachidonoyl-sn-glycero-3-phosphocholine (SAPC; 8), 1-stearoyl-2-arachidonoyl-sn-glycero-3-phosphoethanolamine (SAPE; 14), 1-stearoyl-2-oleoyl-sn-glycero-3-phosphoethanolamine (SOPE; 6), 1-stearoyl-2-arachidonoyl-sn-glycero-3-phospho-L-serine (SAPS; 8), 1-stearoyl-2-linoleoyl-sn-glycero-3-phosphocholine (SLPC; 8), 1-stearoyl-2-arachidonoyl-sn-glycero-3-phosphoinositol (SAPI; 2) and cholesterol (28).

Quantifying spontaneous translocations

The rate constant, k, for translocation across the bilayer is calculated from unbiased MD simulations of spontaneous trans-bilayer solute crossing as the ratio of the total number of transport events observed during a simulation by the simulation time:

$$k = \frac{\#}{t} \qquad \text{(Equation S1)}$$

Transport events are captured by tracking the progress of individual molecules through planes perpendicular to the bilayer normal located at either interface ($\# = \#_{up} + \#_{down}$).

The accurate counting of transport event i ($\#_i$) is non-trivial. To that extent, we define planes for start and end positions for complete transitions. The planes (**Figure 1**) need to satisfy the following criteria: solutes are counted as crossing only when, (i) the transition originates in the bulk region ($z_i < -3.0$ nm or $z_i > 3.0$ nm), as well as (ii) the solute trajectory concludes in the other bulk region of the box ($z_f > 3.0$ nm or $z_f < -3.0$ nm). This criterion ensures that counted events obey a strict distance cutoff criterion. Secondly, molecules that cross the box via the periodic boundary conditions are excluded from the count. Thirdly, incomplete crossings or non-true bulk-to-bulk transitions are excluded.

In order to ensure the concept of bulk-to-bulk transition is obeyed rigorously, we consider the physical properties of the system as a function of temperature. Bilayer thickness is temperature-dependent, with thickness range of ~4.0 nm between 310 K and 440 K (**Table S3**). In addition, the solutes are not point particles, but have significant diameters along their principal axis (**Table S1**;

ranging between 0.5 - 2.0 nm). Thus, in order to be able to define events (#) rigorously, a cutoff criterion of -3.0 nm to 3.0 nm (range of 6.0 nm) is needed to accommodate these observations. Shorter, less rigid definitions of the cutoff (-2.0 nm to 2.0 nm) resulted in overcounting of transition events. Based on the position of the phosphorous groups of the lipid bilayer (**Table S3**), solutes are therefore required to cross the bilayer from an origin 1.0 nm from the bilayer, enter and exit the bilayer, and transition 1.0 nm further ahead of the bilayer, in order to be counted.[3]

The convergence criterion for the rate constant k is two-fold. Firstly, we check for plateau in the value of k for each solute (**Figure S3**), and second, we calculate the numerical gradient from a forward difference expression (Equation S2). The value of k is converged when the gradient descends below 0.004 (dk/dt < 0.004) (**Figure S4**).

$$\frac{dk}{dt} = \frac{k(i+1) - k(i)}{\Delta t} \qquad \text{(Equation S2)}$$

The solute permeability P (cm s^{-1}) is related to the net solute flux J (# cm^{-2} s^{-1}) through a membrane patch by:

$$J = P \cdot \Delta C \qquad \text{(Equation S3)}$$

Where $\Delta C = C_o - C_i$, and C_i (# m^{-3}), C_o (# m^{-3}) are the concentrations on either side of the membrane. Due to pressure coupling, the box volume, V, and area of the bilayer patch, A, will vary during the simulation and need to be averaged.

The permeability is obtained from equation 3, by calculation the flux J. The flux is calculated as the ratio of the frequency k (s^{-1}) per unit molar area ($N_A A$; mol nm^2):

$$J = \frac{k}{N_A A} \qquad \text{(Equation S4)}$$

This leads to a permeability expression of $P = k / N_A AC$. Two caveats are introduced to obtain a final expression for the permeability. However, to be able to compare to experimental measurements, the total flux is divided by 2 as the simulations capture bi-directional flux, such that flux equals the upward plus downward flux ($J = J_{up} + J_{down}$). This results in the final expression for permeability (cm s^{-1}) as:

$$P_{sim} = \frac{k}{2N_A AC} \qquad \text{(Equation S5)}$$

It should be noted that these assumptions are different from experimental calculations, firstly, because *in vitro* assays measure flux in one direction only, and secondly, for *in silico* calculations, we assume that the transport via the cytosol (**Figure 1A**) is fast compared to transport across the cell membrane:

$$k_{BBB} \ll k_{cytosol} \qquad \text{(Equation S6)}$$

Free-energy curves (440 K) and grouping of solutes

The free-energy surface (FES) from our unbiased MD simulations is calculated by, firstly, binning the positions of solute i onto a 1-dimensional probability distribution P(z) along the z-coordinate

variable x (**Figure 2.B**). The free-energy $F(z)$ is calculated by a Boltzmann reweighting of the probability distribution:

$$F(z) = -kTlog(P) \quad \text{(Equation S7)}$$

We describe the parameter library (n(X) = 13) that went into our search. In **Table S1**, a select number of physicochemical parameters of the library of N = 24 molecules are presented. Such parameters include the molecular mass (MW; g mol^{-1}), the diameter of the solute (Å), the number of hydrogen-bond donors (H_{donor}), acceptors (H_{accept}), the octanol-water partition coefficient (logP_{oct}), the dipole moment (Debye), and polar surface area (PSA; Å^2). In **Table S6**, the simulation parameters extracted from the N = 24 unbiased MD simulations for solutes across the BBB are presented, namely: (i) the drug residence time inside the BBB bilayer (t_{res}), which is a measure of lipophilicity, (ii) the rate of attempted transitions, calculated as the number of failed crossings ($\#_{failed}$) normalized by simulation time (t_{sim}), (iii) the percentage of successful transitions, calculated as $\#_{succesful}$ / $\#_{total}$, where $\#_{total} = \#_{succesful} + \#_{failed}$, (iv) k (ns^{-1}), the rate constant for BBB transbilayer crossing for particular solute i, with error bound by one standard deviation σ (k) (ns^{-1}), (v) parameters ΔG_1, ΔG_2, ΔG_3, where the maximum barrier encountered among ΔG_1, ΔG_2 or ΔG_3 is reported as ΔG_{max}.

Model Validation

Validation of the bilayer model

To validate our model of the bilayer membrane, we first considered the physical properties of the system as a function of temperature. First, bilayer thickness was shown to be temperature-dependent between 310 K (4.44 nm) and 440 K (3.84 nm) (**Table S3**), consistent with the thinning of bilayers at higher temperatures.[20, 25] Secondly, we showed that at 310 K, the lateral diffusivity for POPC and SOPE lipids, as well as individual area-per-lipid (APL) measurements of POPC and SOPE, were close to experimentally determined values (**Table S4**). Finally, we showed that the temperature dependence of the lipid diffusion coefficients and the area-per-lipid (**Fig. S5**) were also consistent with previous MD simulations.[20] Having validated the biophysical properties of the bilayer membrane, we verified that the translocation frequency k at 440 K was independent of the solute concentration, bilayer area, and volume of the simulation box for selected solutes (**Table S5 and Fig. S6**).

Force field potentials

In atomistic simulations, the quality of the force field potentials of the solutes is a key issue in the accuracy of the simulations. As described above, we cannot rely solely on experimental values of permeability to diagnose possible errors in the simulation potential due to the discrepancies between *in vitro* and *in vivo* measurements. The CGenFF penalty score (p_{charge}, $p_{parameter}$; **Table S11**) measures the appropriateness of the force field partial charges (p_{charge}) and force field parameters ($p_{parameter}$), where a larger penalty indicates a poorer analogy to quantum mechanical calculations. There was no correlation (R^2 = 0.005) between the CGenFF penalty parameter and the apparent difference in permeability between simulations and *in vitro* values (i.e. log$P_{sim,310K}$ - logP_{app}) (**Fig. S13**). This suggests that the potentials (**Table S12**) are not the main contributing factor to the differences between simulated and experimental permeabilities.

In addition to the force field parameter assignment, the results could be influenced by the lack of polarizability effects in the CGenFF force field. Classical force fields including CHARMM, AMBER, and GROMOS can only account for environment polarizability in a static manner,[26] and do not capture the polarizability of solutes in changing and its changing environment, such as during the transfer from polar to non-polar environments. These contributions for are likely to be significant for translocation across lipid bilayers. The use of polarizable force fields,[27] could be an important improvement on the current methods, and this can be achieved with the empirical Drude polarizable force field[28-30] with the FFParam package for molecular solutes,[31] or the AMOEBA polarizable force field.[32]

SI Figures

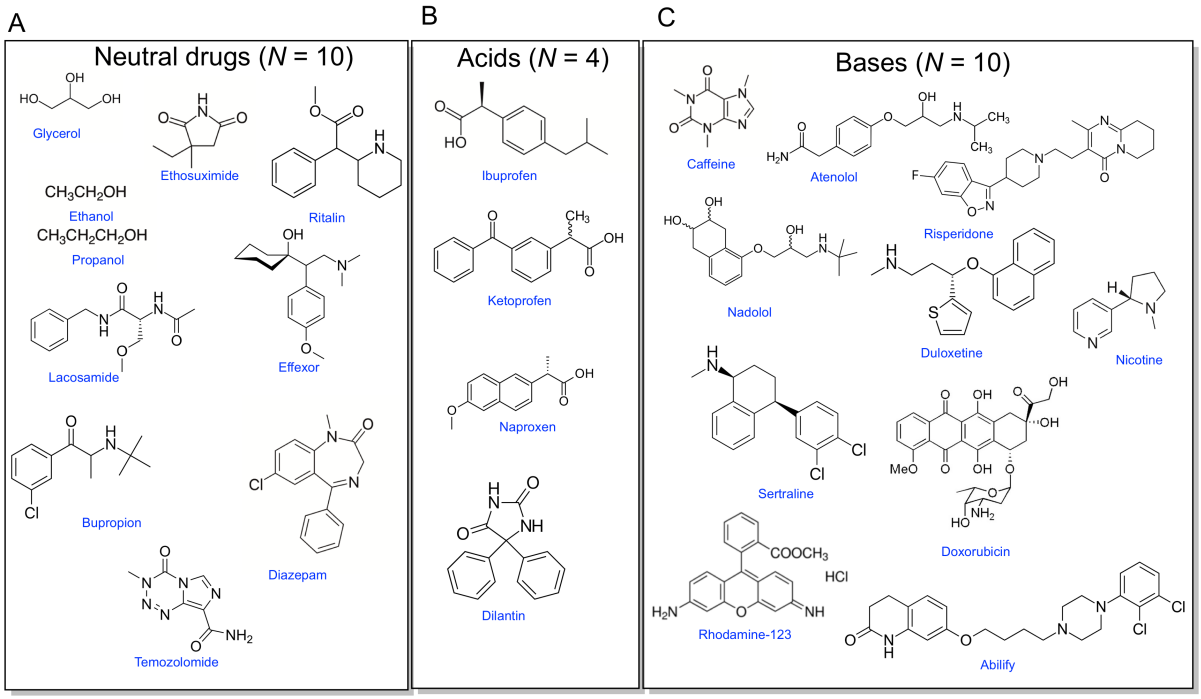

Figure S1. Chemical structures of the library (N = 24) of molecules used a representation of the BBB drug space. This library spans compounds possessing *in vitro* 2D and 3D permeabilities (P_{app}) in the range from 10^{-7} cm s^{-1} to 10^{-3} cm s^{-1}. The library spans compounds (A) that at pH = 7 are neutral (non-ionized) molecules (N = 24), (B) cationic (acidic) compounds (N = 4), and (C) anionic (basic) compounds (N = 10).

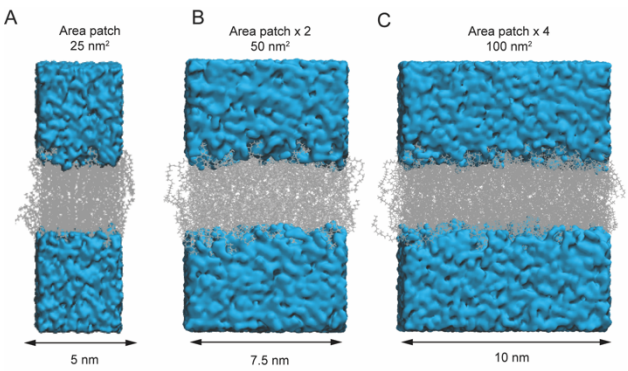

Figure S2. Membrane area. The membrane patches consist of (A) 96 lipids (approximately 25 nm^2), (B) 192 lipids (approximately 50 nm^2; double area box) and (C) 384 lipids (approximately 100 nm^2; quadruple area box), respectively. Decreasing the size of the lipid patch did not impact on the accuracy of P_{sim}.

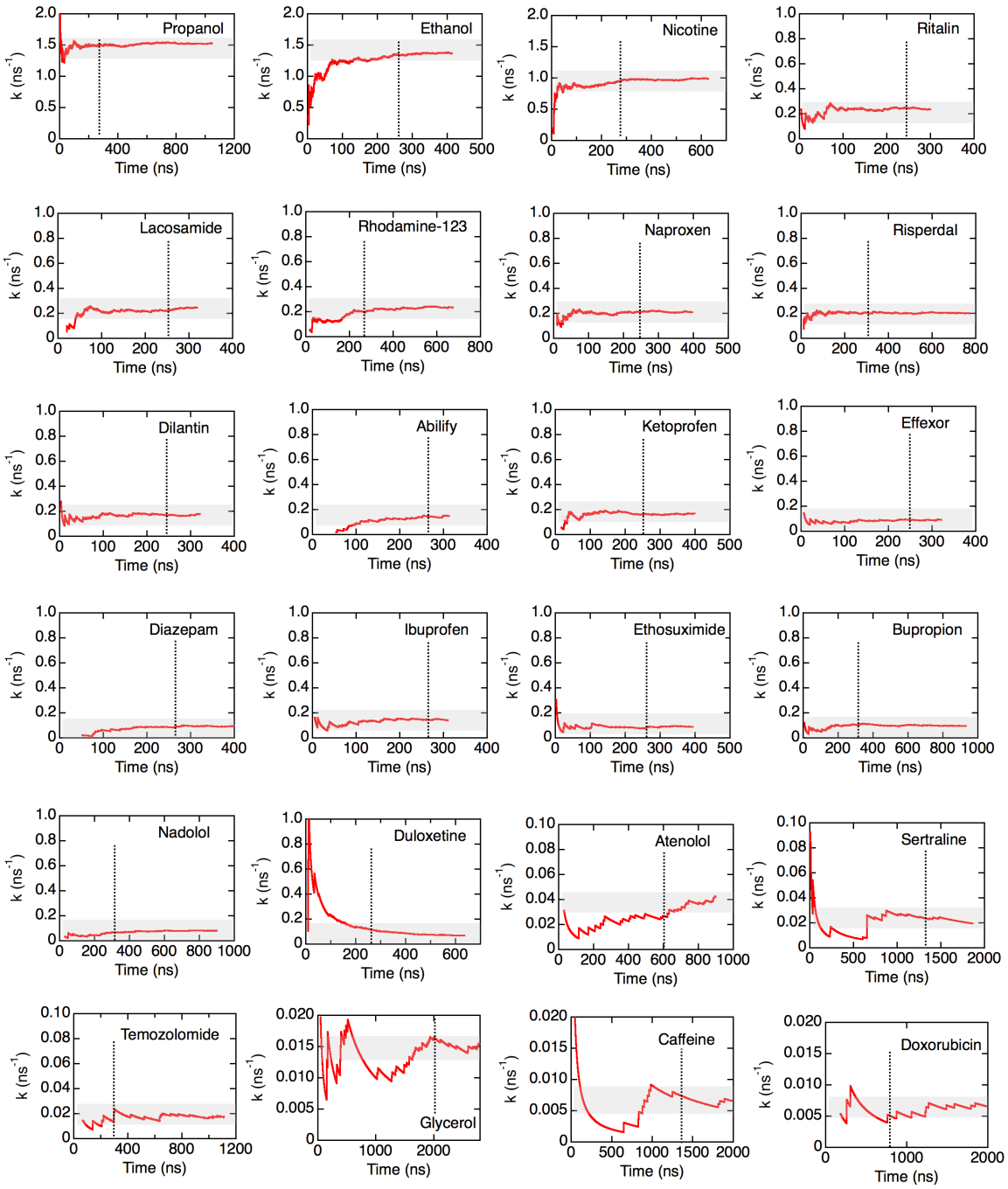

Figure S3. Translocation frequency (*k*) convergence as a function of simulation time (ns) for a library of (*N* = 24) solutes ranked by value of *k*. The number of events ($\#_{events}$) is defined as the number of times a molecule spontaneously crosses the BBB membrane from – 3 nm to + 3 nm or vice-versa ($\#_{events} = \#_{up} + \#_{down}$). The frequency $k = \#_{events} / t_{sim}$. A plateau in *k,* indicating convergence of the estimate, is checked by the forward difference gradient reduced to a threshold of dk/dt < 0.004.

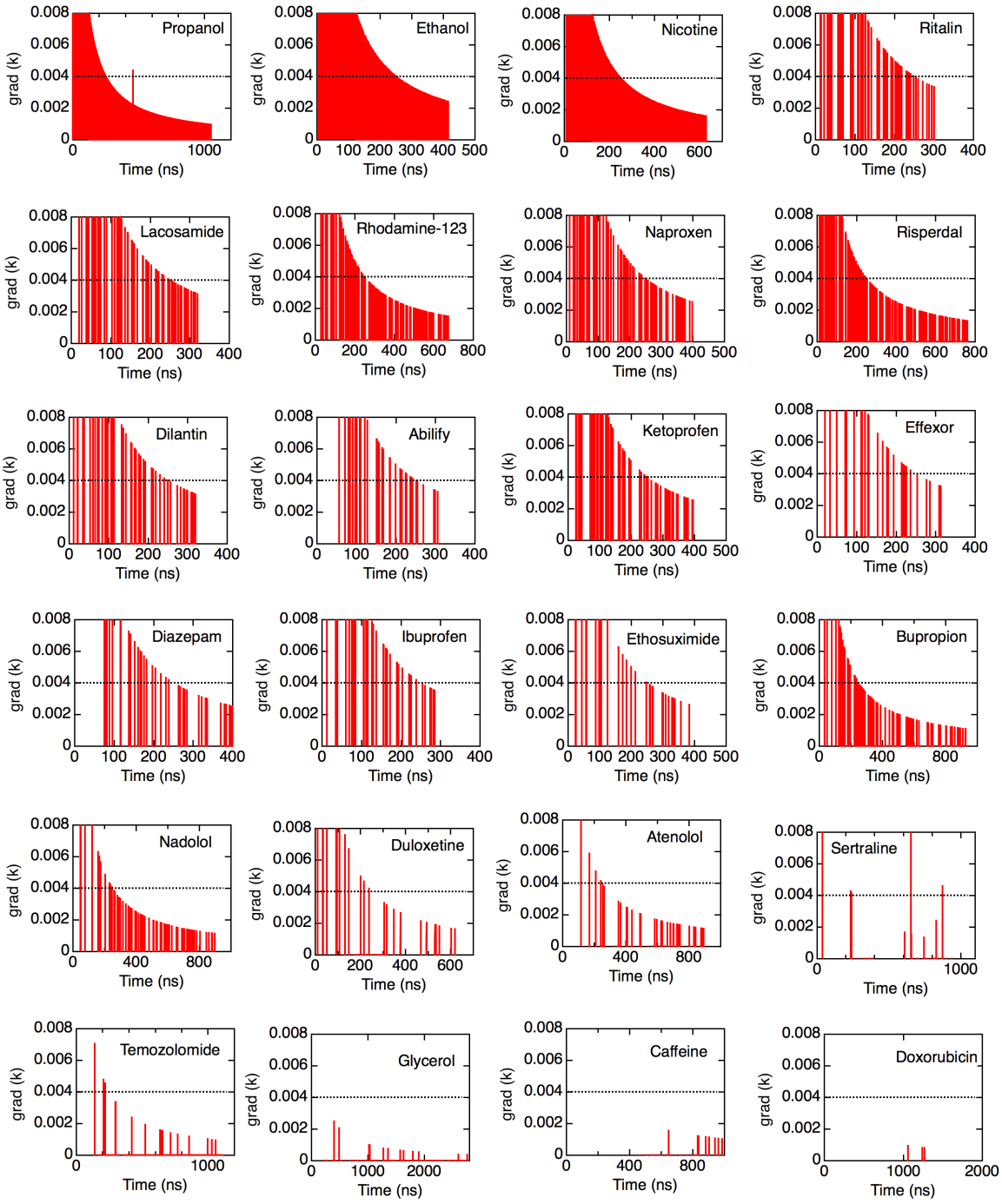

Figure S4. Convergence threshold for the numerical evaluation of the rate constant *k* based on forward-difference gradient, following the ranking in Figure S3. The numerical gradient of *k* is defined as a forward differences estimate of grad = ($k(i + 1)$ - $k(i)$) / Δt, where $\Delta t = t(i+1) - t(i)$. A hard convergence criterion is imposed, where *k* is deemed converged if and only if grad < 0.004.

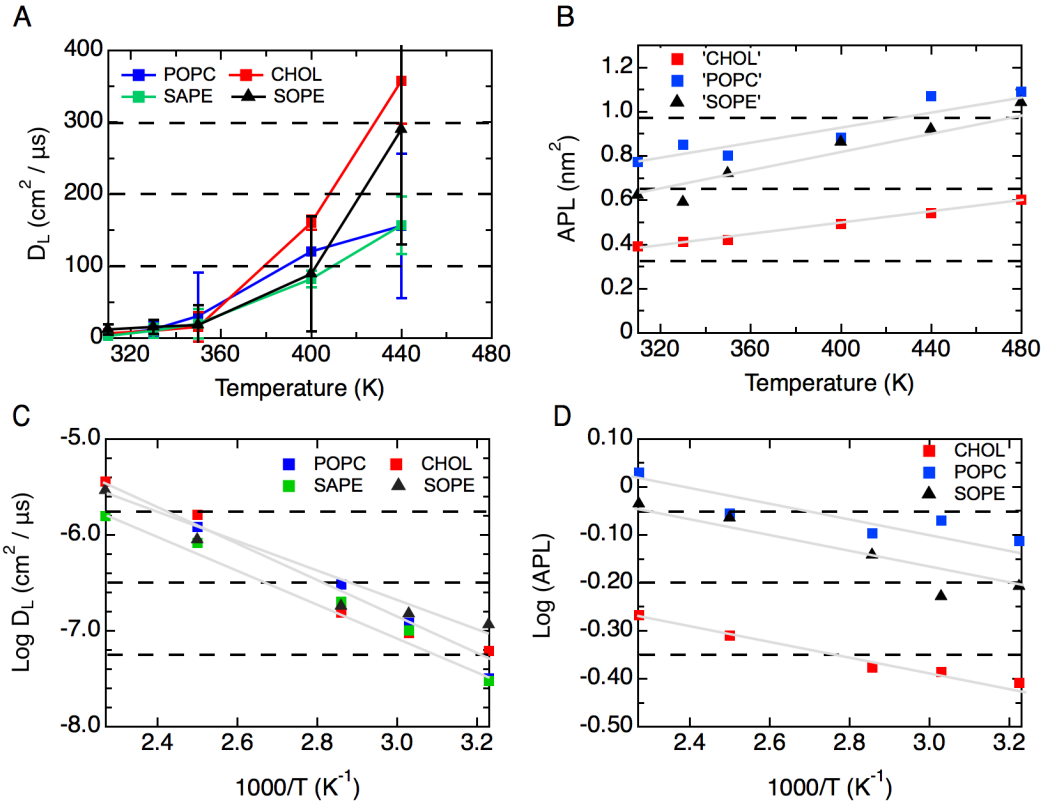

Figure S5. **Temperature dependence of the diffusion coefficients and the area-per-lipid of individual lipids of the apical lipid bilayer**. (A) The average lipid diffusion coefficient in the plane of the membrane, $D_L(T)$, calculated by averaging the diffusion of heavy atoms for all lipid species in the bilayer for lipids POPC (blue), SAPE (green), SOPE (black) and cholesterol (red). (B) Area per lipid for POPC (blue), SOPE (black) and cholesterol (red). (C,D) Log plot of $D_L(T)$ and APL as a function of temperature.

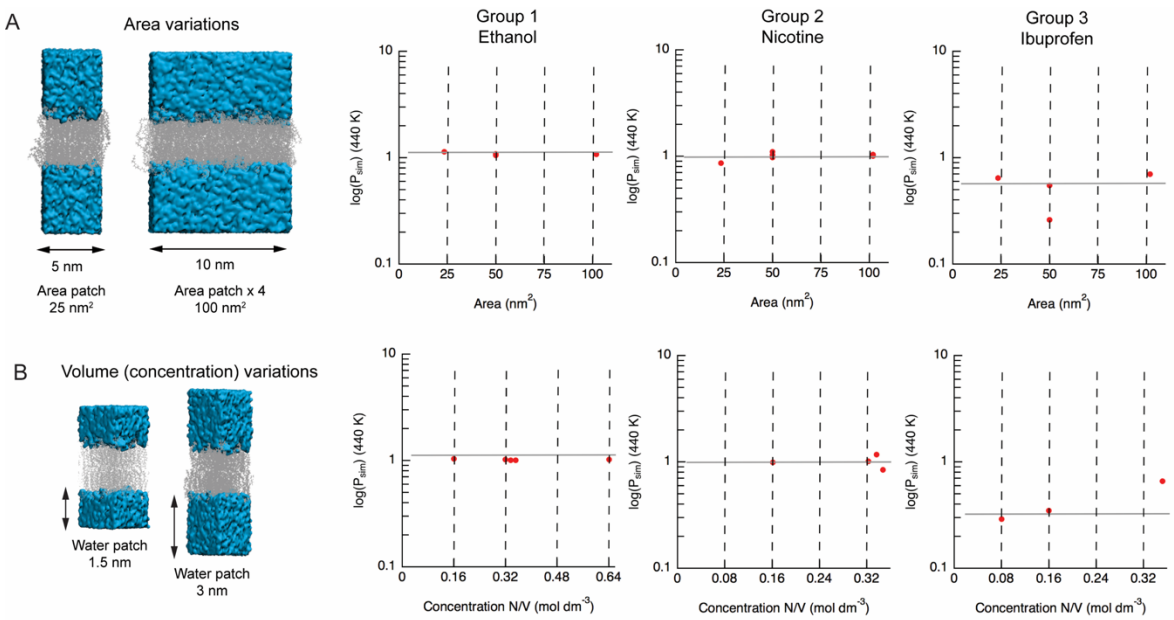

Figure S6. Consistency of P_{sim} values obtained from (A) variations in membrane area and (B) variations in the water volume. The respective P_{sim} values reveal it is possible to calculate a permeability across all three groups of molecules utilizing the smallest patch (25 nm^2 area) or the smallest water box (solute concentration of 0.16 mol dm^{-3}), thereby accelerating the sampling without loss of accuracy. The systems contain N = 20, 40 or 80 molecules in box, rendering the solute concentrations of 0.16, 0.32 or 0.64 M.

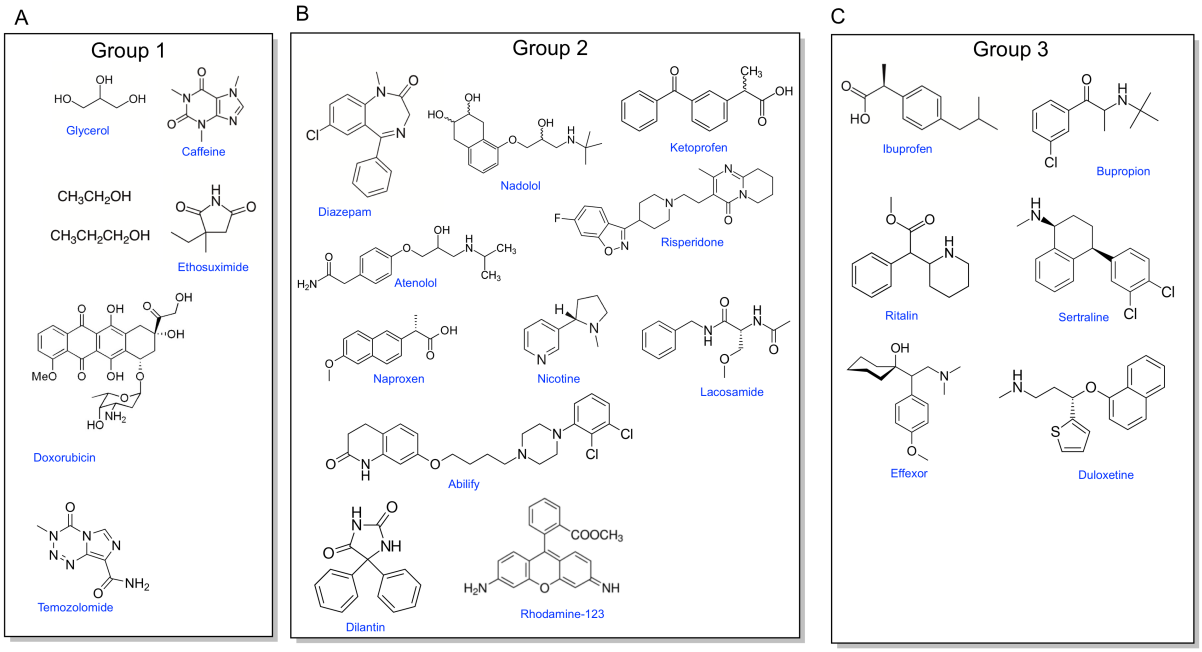

Figure S7. Chemical structures of the library (*N* = 24) arranged by energy-clustered groups 1-3. (A) group 1 cluster, containing ethanol, propanol, glycerol, caffeine, doxorubicin and temozolomide. (B) group 2 cluster, containing diazepam, nadolol, ketoprofen, atenolol, risperidone, abilify, dilantin, and rhodamine-123. (C) Group 3 cluster spanning ibuprofen, bupropion, Ritalin, sertraline, Effexor, and duloxetine.

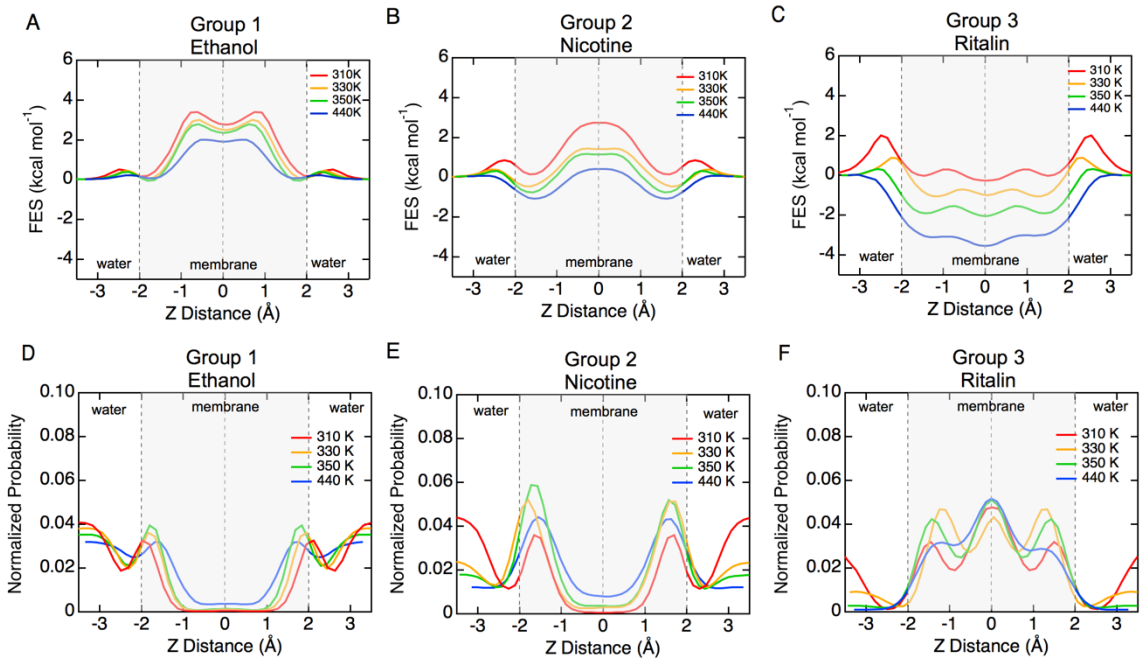

Figure S8. **Temperature-dependence of the transbilayer free-energy surfaces (FES) and probability density from solute density for three representative molecules of each energy-binned groups**. (A-C) Free-energy surfaces (FES). The molecules are ethanol (group 1), nicotine (group 2), and ritalin (group 3), and simulations were performed at 310 K (red), 330 K (orange), 350 K (green) and 440 K (blue). (D-F) Normalized probability density for spontaneous transbilayer solute crossing at 310 K (red), 330 K (orange), 350 K (green) and 440 K (blue).

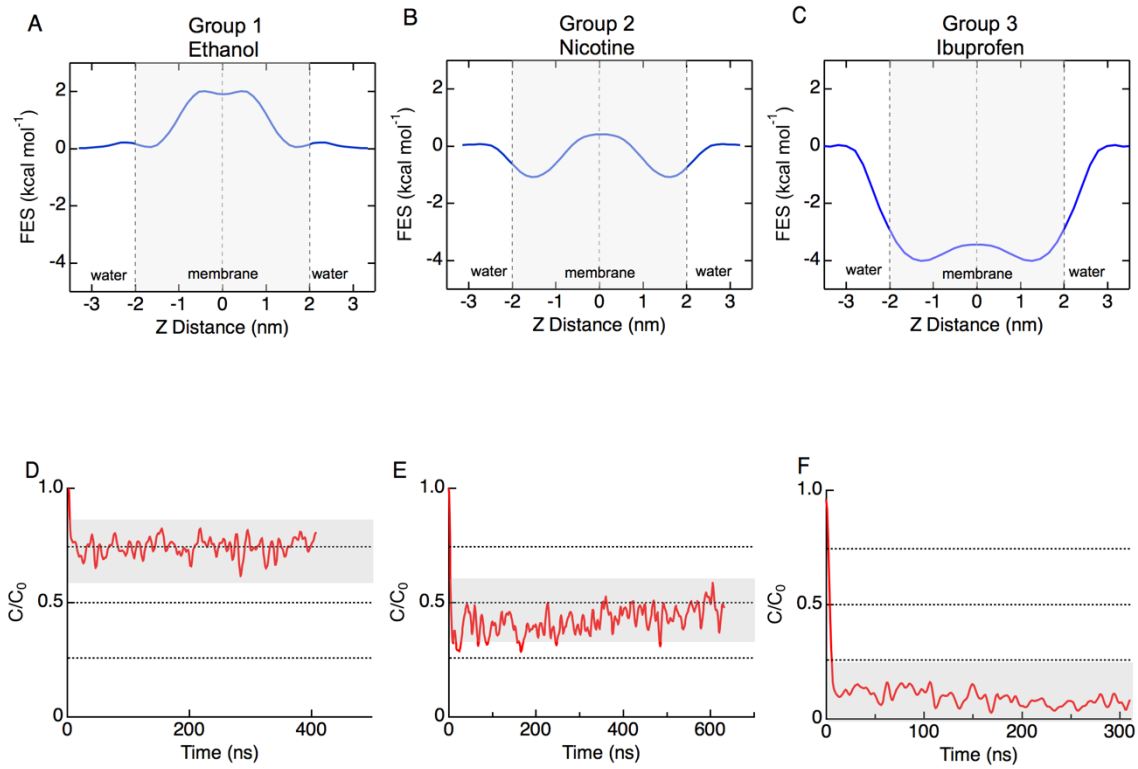

Figure S9. Solute steady-state concentration (C/C_0) with associated free-energy surface (FES) for group 1-3 molecules. (A-C) Free-energy surfaces (FES) at 440 K. (D-F) Fraction of solute molecules within the bilayer. Group 1 molecules (ethanol) are polar drugs with energy maximum at the bilayer hydrophobic core and majority population in the bulk at steady state, such that there is a low probability of finding a molecule in the core. Group 2 molecules (nicotine) are polar drugs with an energy maximum at the bilayer hydrophobic core and have an associated low probability of residing in the core. Group 3 molecules (ibuprofen) are lipophilic drugs with an energy minimum at the bilayer hydrophobic core, and an associated near-zero probability of finding a molecule outside the bilayer core. Since there are relatively few molecules in the simulation, the concentration of the solute in bulk water decreases to a steady state. For all groups, the number of solute molecules in the membrane depends on the degree partitioning (lipophilicity), and the permeability, i.e. the number of molecules crossing the bilayer per unit time.

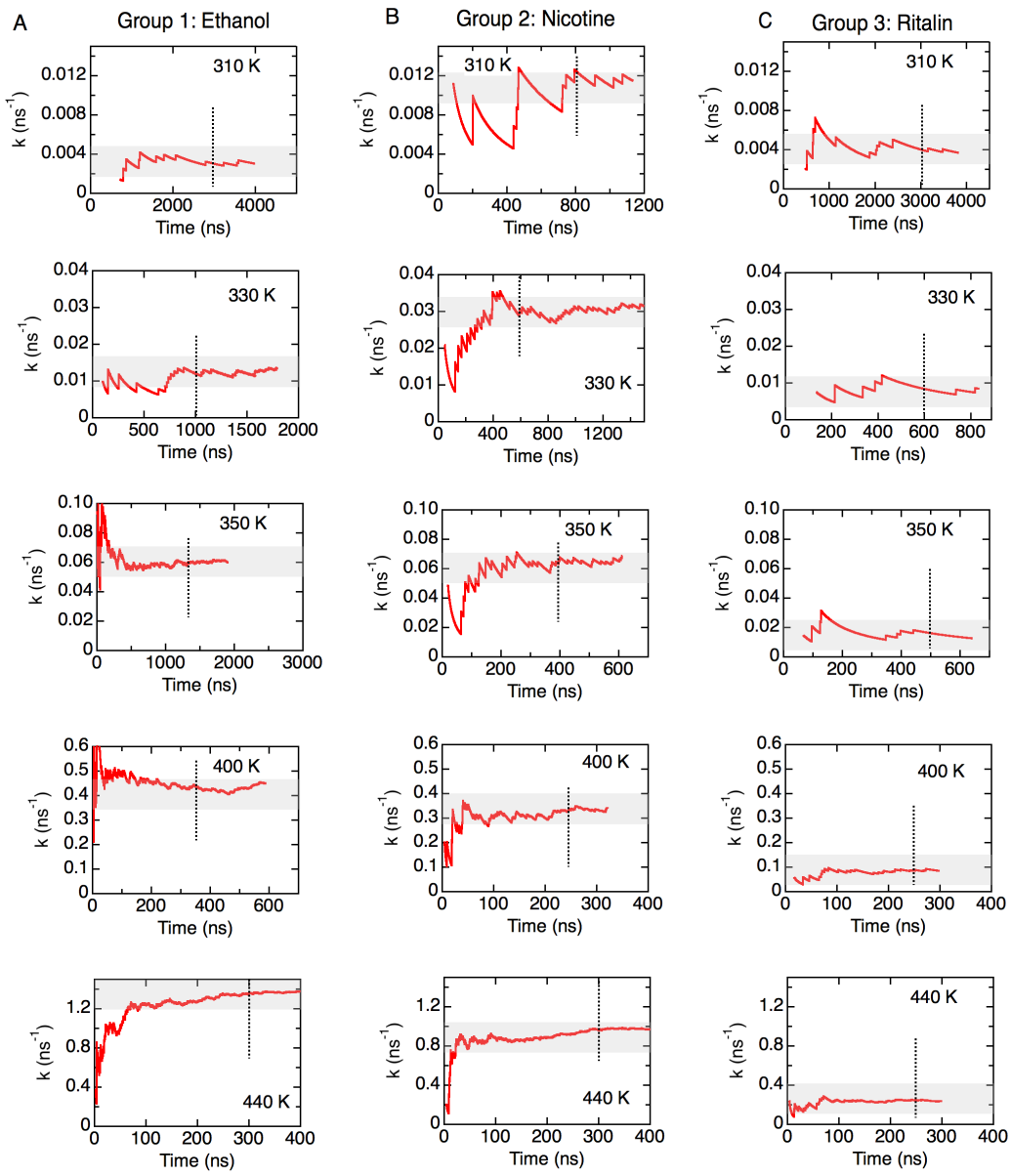

Figure S10. Spontaneous trans-bilayer transition rate (*k*) convergence as a function of simulation time (ns) for three energy-clustered groups of molecules. The molecules are ethanol (A; group 1), nicotine (B; group 2), and ritalin (C; group 3), and the rate constant *k* was evaluated at temperatures 310 K, 330 K, 350 K, 400 K, 440 K. A plateau in *k,* indicating convergence of the estimate, is checked by the forward difference gradient reduced to a threshold of grad < 0.004.

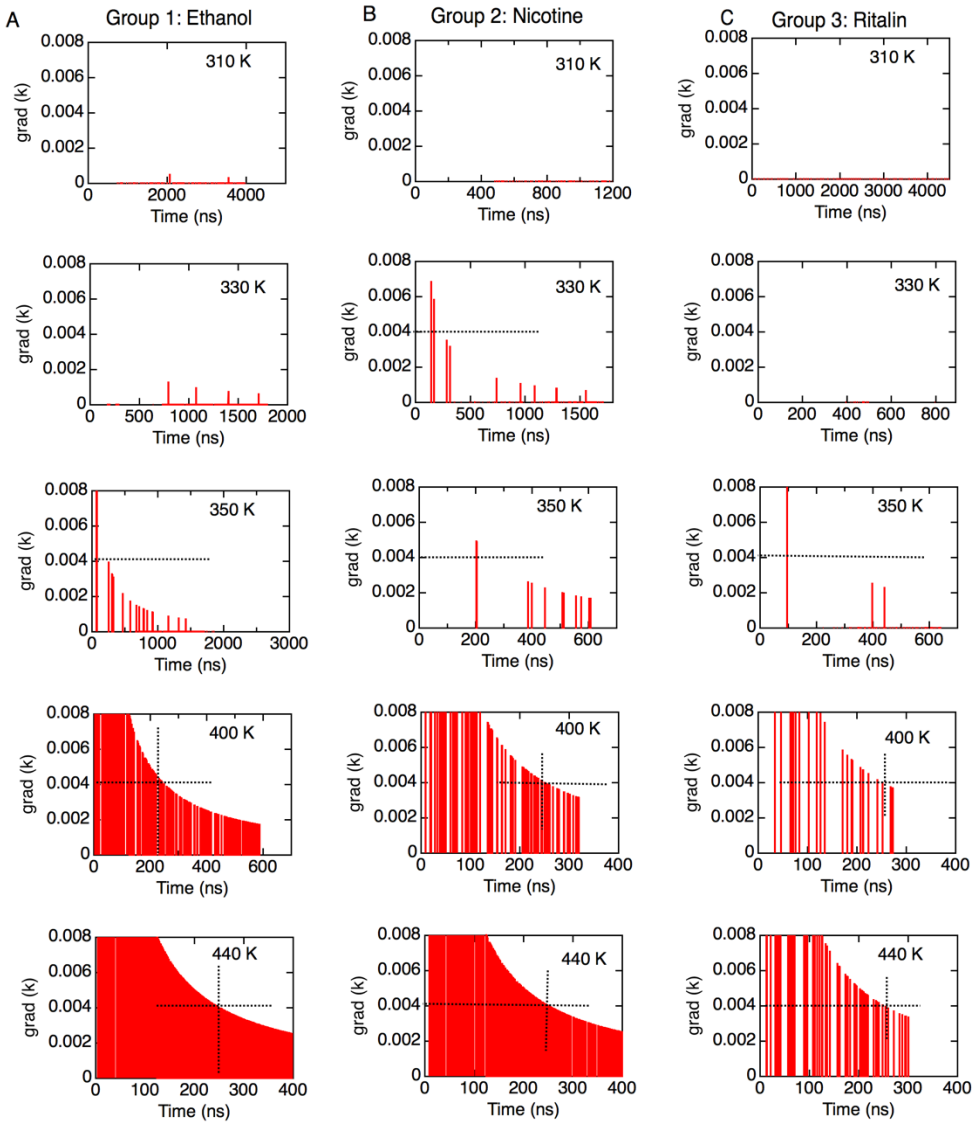

Figure S11. Convergence threshold for the numerical evaluation of the rate constant *k* based on forward-difference gradient. The molecules are ethanol (A; group 1), nicotine (B; group 2), and ritalin (C; group 3), evaluated at temperatures 310 K, 330 K, 350 K, 400 K, and 440 K. The numerical gradient of k is defined as a forward differences estimate of grad = $(k(i + 1) - k(i)) / \Delta t$, where $\Delta t = t(i+1) - t(i)$. A hard convergence criterion is imposed, where k is deemed converged if and only if grad < 0.004.

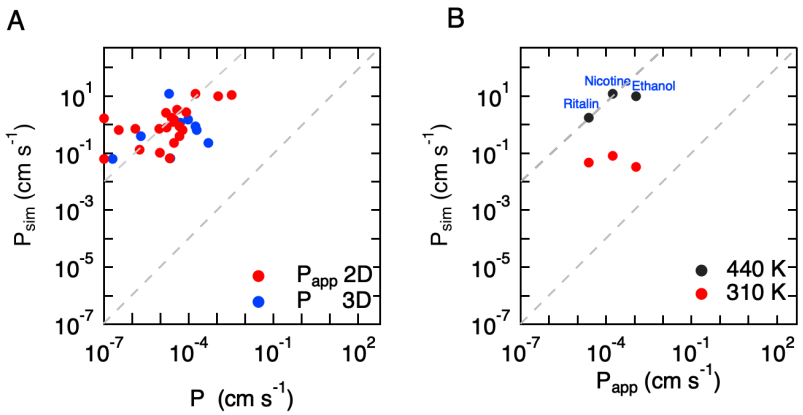

Figure S12. Comparison of permeability values. (A) Permeability calculated from simulations (P_{sim}, at 440K) versus permeability measured in 2D (Papp 2D) and permeability measured in vivo by 3D brain perfusion (P 3D). (B) Permeability calculated from simulations (Psim, at 440K) and extrapolated values at 310 K versus permeability measured in 2D confluent monolayers (Papp 2D).

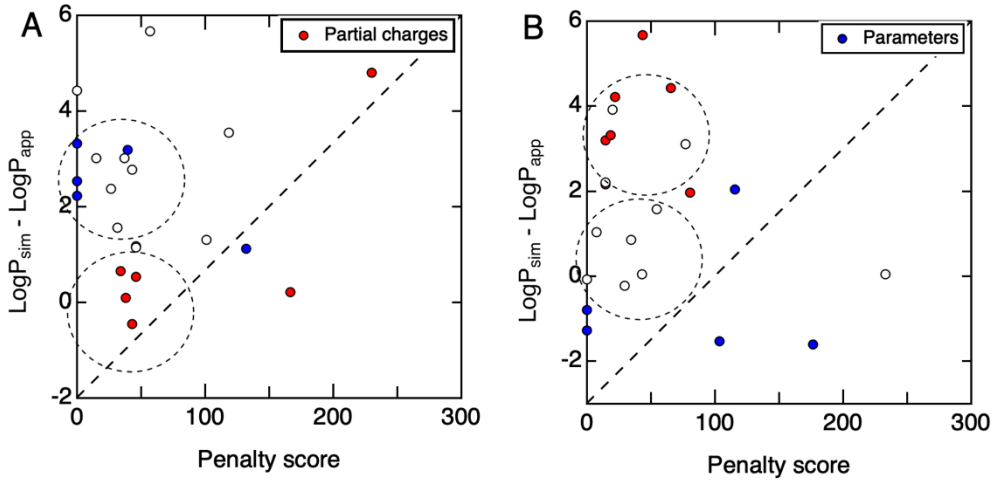

Figure S13. Difference in simulated and experimental 2D permeability ($\log P_{\text{sim, 310 K}} - \log P_{\text{app}}$) **and force field quality of assignment penalty score *p* for charges and bonded parameters** ($p_{\text{charge}}, p_{\text{parameter}}$) **for $N = 23$ molecules**. The plots refer to permeability difference as a function of (A) force field partial charges, and (B) force field bonded parameter assignment. Groups 1, 2, 3: red, white, and blue; respectively, as indicated in Figure S7.

Tables

Table S1. Reference physicochemical parameters for a library of solutes.

Molecule	Group	MW (g mol^{-1})	Diameter (Å)	H_{donor}	H_{accept}	Log *P*	DP (debye)	Polar surf. area
Glycerol	1	92.09	5.3	3	3	-1.8	2.62	60.7
Temozolomide	1	194.1	8.7	1	5	0.4	6.10	106.0
Caffeine	1	194.2	6.4	0	3	-0.07	3.64	58.4
Ethanol	1	46.1	2.7	1	1	-0.31	1.69	20.2
Propanol	1	60.1	4.1	1	1	0.05	1.68	20.2
Doxorubicin	1	543.5	13.6	6	12	1.27	9.12	206
Ethosuximide	1	141.2	6.6	1	2	0.38	1.72	46.2
Atenolol	2	266.3	16.3	3	4	0.16	5.00	84.6
Diazepam	2	284.7	9.5	0	2	2.82	2.65	32.7
Nadolol	2	309.4	15.2	4	5	0.81	5.10	82.0
Lacosamide	2	250.3	12.2	2	3	0.73	1.90	67.4
Abilify	2	448.4	19.3	1	4	4.5	6.01	44.8
Risperdal	2	410.4	17.5	0	6	3.49	5.45	61.9
Rhodamine-123	2	380.8	11.3	2	5	1.06	6.11	87.1
Dilantin	2	252.3	5.8	2	2	2.47	2.73	58.2
Ketoprofen	2	254.3	12.2	1	3	3.12	4.44	54.4
Naproxen	2	230.3	11.6	1	3	3.18	2.25	46.5
Nicotine	2	162.2	6.9	0	2	1.17	1.64	16.1
Ibuprofen	3	206.3	8.1	1	2	3.97	1.64	37.3
Effexor	3	277.0	9.6	1	3	3.2	3.33	32.7
Ritalin	3	233.1	7.3	1	3	2.25	2.13	38.3
Sertraline	3	306.2	8.8	1	1	5.10	3.86	12.0
Duloxetine	3	297.4	11	1	3	4.00	2.18	49.5
Bupropion	3	239.7	8.3	2	4	3.60	1.15	29.1

Table S2. Experimental values of permeability for molecules in groups 1-3. *IH* denotes measurement made in house by authors. *NA* value not known. Two-dimensional (2D) cell culture terminology includes red blood cell (RBC), Madin-Darby Canine Kidney (MDCK) cells, human epithelial colorectal adenocarcinoma (Caco-2) cells and induced pluripotent stem cell (iPSC) line. 3D i*n situ* brain perfusion value given where no 2D value was reported.

Molecule	Group	P_{app} (cm s^{-1})	P_{3D} (cm s^{-1})	P_{app} References	P_{3D} References	Cell line (2D) (T/K)
Glycerol	1	9.50×10^{-6}	-	[33]	-	BMEC [310 K]
Temozolomide	1	1.86×10^{-6}	-	[34]	-	Inference from PAMPA [298 K]
Caffeine	1	2.10×10^{-5}	2.22×10^{-5}	*IH*		MDCK [298 K]
Ethanol	1	1.10×10^{-3}	-	[35]	-	RBC [298 K]
Propanol	1	3.30×10^{-3}	-	[35]	-	RBC [298 K]
Doxorubicin	1	1.00×10^{-7}	2.00×10^{-7}	[36]	[36]	Caco-2 / MDCK [310 K]
Ethosuximide	1	9.00×10^{-6}	-	[37]	-	MDCK [310 K]
Atenolol	2	1.30×10^{-6}	-	[38]	-	Caco-2 [310 K]
Diazepam	2	4.60×10^{-5}	2.00×10^{-6}	[37]	[37]	MDCK [310 K]
Nadolol	2	3.30×10^{-7}	-	[39]	-	Caco-2 [298 K]
Lacosamide	2	1.60×10^{-5}	-	[40]	-	Caco-2 [298 K]
Risperdal	2	3.00×10^{-5}	9.44×10^{-5}	[37]	[37]	MDCK [310 K]
Rhodamine	2	0.80×10^{-7}	-	[41]	-	iPSC [298 K]
Dilantin	2	2.70×10^{-5}	5.00×10^{-5}	[37]	[37]	MDCK [310 k]
Ketoprofen	2	8.00×10^{-5}	-	[42]	-	Caco-2 [298 K]
Naproxen	2	3.90×10^{-5}	-	[43]	-	Caco-2 [298 K]
Nicotine	2	1.78×10^{-4}	2.02×10^{-5}	[44]	[45]	Caco-2 / MDCK
Ibuprofen	3	2.70×10^{-5}	-	*IH*	-	MDCK [298 K]
Effexor	3	6.00×10^{-5}	1.88×10^{-4}	[36]	[46]	Caco-2 / MDCK [310 K]
Ritalin	3	2.47×10^{-5}	-	[47]	-	MDCK [310 K]
Sertraline	3	2.1×10^{-6}	4.99×10^{-4}	[37]	[37]	MDCK [310 K]
Duloxetine	3	1.66×10^{-5}	-	[36]	-	Caco-2 / MDCK [310 K]
Bupropion	3	4.75×10^{-5}	1.69×10^{-4}	[37]	[37]	MDCK [310 K]

Table S3. Position of phosphorous (P) atom in the BBB bilayer. Error range is for average in lower and upper leaflets.

	T (K)	Avg P position (nm)	Error range (σ) (nm)
Standard box	440	± 1.92	0.05-0.2
	310	± 2.22	0.04-0.14
Double box	440	± 1.97	0.2-0.3
	310	± 2.24	0.08-0.12

Table S4. Comparison of lipid lateral diffusivity and lipid area-per-lipid (APL) to reference values.

Property	Simulation	Reference
POPC Diffusivity (10^{-8} cm^2/s)	3.15 ± 0.8	3.2 - 5.68 ‡
SOPE Diffusivity (10^{-8} cm^2/s)	11.5 ± 7.3	2.0 – 4.0 †
POPC APL (nm^2)	0.77 ± 0.05	0.643*
SOPE APL (nm^2)	0.62 ± 0.02	0.590*
CHOL APL (nm^2)	0.39 ± 0.04	0.393*

‡ Gurtovenko, A.A.;Vattulainen, I., "Membrane Potential and Electrostatics of Phospholipid Bilayers with Asymmetric Transmembrane Distribution of Anionic Lipids," *J Phys Chem B* **2008**, 112 (15), 4629-4634.
† Pitman, M.C.; Suits, F.; Gawrisch, K.; Feller, S.E., "Molecular dynamics investigation of dynamical properties of phosphatidylethanolamine lipid bilayers," *J Chem Phys* **2005**, 122 (24), 244715.

Table S5. Ethanol permeability (440 K) as a function of concentration. The P_{sim} is reported to be independent of concentration of simulation.

N molecules	Water (nm^3)	t_{conv} (ns)	k (ns^{-1})	P_{sim} (cm s^{-1})
1	50	250	0.06	8.5
20	100	245	1.36	10
20	100	245	1.32	9.7
20	400	245	0.65	10.7
40	400	250	1.18	9.8
80	400	257	2.55	10.6
40	800	248	1.23	10.2
80	800	249	2.46	10.3

Table S6. Kinetic and thermodynamic parameters extracted from simulations of the library of solutes (440 K). The energy-based grouping is indicated, the time of simulation, the residence time in the bilayer (t_{res} in ns), the number of failed transitions per simulation time ($\#_{failed}$ / t_{sim}), the % of transitions that are successful in crossing the BBB, the rate constant *k* and corresponding error as standard deviation ($\sigma(k)$), and the values for free-energy barriers ΔG_1 (escape barrier from hydrophobic core), ΔG_2 (polar molecule barrier), ΔG_3 (transverse minimum crossing).

Molecule	Group	t_{sim} (ns)	t_{res} (ns)	$\#_{failed}$ / t_{sim} (ns^{-1})	% transition	*k* (ns^{-1}) ± s(k) (ns^{-1}) 440 K	ΔG_1 (kcal mol^{-1})	ΔG_{max} or ΔG_2 (kcal mol^{-1})	ΔG_3 (kcal mol^{-1})
Glycerol	1	2838	0.567	296.2	0.0062	0.01370 ± 0.002	0.0	6.0	6.0
Temozolomide	1	1317	0.783	134.7	0.0147	0.01780 ± 0.002	-1.2	5.7	5.7
Caffeine	1	1000	1.437	105.0	0.0086	0.00685 ± 0.001	-1.3	5.6	5.6
Ethanol	1	416	0.519	463.4	0.2927	1.35800 ± 0.010	0.0	2.1	2.1
Propanol	1	1167	0.807	319.7	0.4718	1.51190 ± 0.020	-0.4	1.4	1.4
Doxorubicin	1	2000	1.580	44.5	0.0146	0.00658 ± 0.002	-0.1	3.3	3.3
Ethosuximide	1	396	1.154	135.0	0.0635	0.08690 ± 0.005	-0.2	3.6	3.6
Atenolol	2	904	2.504	16.1	0.2599	0.03850 ± 0.002	-2.3	2.6	2.6
Diazepam	2	400	3.004	22.3	0.6253	0.05640 ± 0.020	-2.6	2.9	2.9
Nadolol	2	904	2.917	10.8	0.7196	0.07140 ± 0.010	-2.8	3.2	3.2
Lacosamide	2	320	2.085	58.2	0.4227	0.23500 ± 0.010	-1.7	2.3	2.3
Abilify	2	270	4.610	5.3	3.0956	0.13610 ± 0.010	-3.1	3.1	-1.1
Risperdal	2	775	4.134	11.4	1.7025	0.20100 ± 0.003	-2.9	2.9	-1.5
Rhodamine-123	2	675	3.433	15.7	1.4565	0.22200 ± 0.010	-2.8	2.8	-1.8
Dilantin	2	323	3.448	9.2	1.8899	0.16650 ± 0.005	-3.4	3.4	2.0
Ketoprofen	2	400	3.897	2.2	7.0213	0.16100 ± 0.003	-3.1	3.1	1.0
Naproxen	2	400	3.732	3.3	5.8574	0.20000 ± 0.020	-2.7	2.7	0.9
Nicotine	2	503	1.420	150.5	0.8167	0.97000 ± 0.010	-1.1	1.1	1.5
Ibuprofen	3	400	4.427	4.9	2.1404	0.14410 ± 0.003	-4.0	4.0	0.6
Effexor	3	323	5.194	2.4	6.3170	0.08780 ± 0.002	-4.0	4.0	-0.6
Ritalin	3	301	3.469	7.4	4.5840	0.23960 ± 0.005	-3.5	3.5	0.3
Sertraline	3	951	8.554	0.6	4.1335	0.02380 ± 0.002	-1.1	1.1	1.5
Duloxetine	3	636	5.943	1.2	5.3915	1.46600 ± 0.030	-1.1	1.1	1.5
Bupropion	3	937	4.230	3.2	2.8296	0.09250 ±0.010	-1.1	1.1	1.5
Total (ns)		18555							

Table S7. Kinetic parameters extracted from simulations of the library of solutes (440 K) ranked by frequency (*k*).

Molecule	Group	t_{sim} (ns)	$\#_{trans}$/μs	k (ns^{-1})	Area (nm^2)	Conc. (mol dm^{-3})	P_{sim} (cm s^{-1})	P_{app} (cm s^{-1})
Doxorubicin	1	2000	7	0.00658	31.9	3.52×10^{-1}	6.34×10^{-2}	1.00×10^{-7}
Caffeine	1	1000	9	0.00685	31.9	3.52×10^{-1}	6.60×10^{-2}	2.10×10^{-5}
Glycerol	1	2838	18	0.01370	31.9	2.70×10^{-1}	1.01×10^{-1}	9.50×10^{-6}
Temozolomide	1	1317	20	0.01780	31.9	3.54×10^{-1}	1.32×10^{-1}	1.86×10^{-6}
Sertraline	3	951	27	0.02380	31.9	3.52×10^{-1}	2.29×10^{-1}	5.00×10^{-4}
Atenolol	2	904	42	0.03850	31.9	2.70×10^{-1}	6.99×10^{-1}	1.30×10^{-6}
Duloxetine	3	636	66	1.46600	31.9	3.19×10^{-1}	1.41×10^{1}	1.66×10^{-5}
Nadolol	2	904	79	0.07140	33.9	1.35×10^{-1}	6.48×10^{-1}	3.30×10^{-7}
Ethosuximide	1	396	86	0.08690	35.3	3.41×10^{-1}	7.09×10^{-1}	9.00×10^{-6}
Bupropion	3	937	94	0.09250	33.9	2.70×10^{-1}	8.92×10^{-1}	4.75×10^{-5}
Ibuprofen	3	400	108	0.14410	19.7	3.74×10^{-1}	1.60×10^{0}	2.70×10^{-5}
Diazepam	2	400	140	0.05640	31.9	3.52×10^{-1}	3.88×10^{-1}	4.60×10^{-5}
Effexor	3	323	164	0.08780	31.9	3.52×10^{-1}	6.49×10^{-1}	6.00×10^{-5}
Ketoprofen	2	400	165	0.16100	31.9	3.52×10^{-1}	2.72×10^{0}	8.00×10^{-5}
Dilantin	2	323	176	0.16650	36.8	1.34×10^{-1}	1.23×10^{0}	2.70×10^{-5}
Risperdal	2	775	197	0.20100	36.8	1.34×10^{-1}	1.49×10^{0}	3.00×10^{-5}
Naproxen	2	400	208	0.20000	20.0	3.33×10^{-1}	3.37×10^{0}	3.90×10^{-5}
Rhodamine-123	2	675	233	0.22200	31.9	2.35×10^{-1}	1.64×10^{0}	0.80×10^{-7}
Lacosamide	2	320	247	0.23500	31.9	3.52×10^{-1}	2.65×10^{0}	1.60×10^{-5}
Ritalin	3	301	359	0.23960	31.9	3.52×10^{-1}	1.77×10^{0}	2.47×10^{-5}
Nicotine	2	503	1240	0.97000	31.9	2.70×10^{-1}	1.21×10^{1}	1.78×10^{-4}
Ethanol	1	416	1361	1.35800	31.9	2.70×10^{-1}	9.99×10^{0}	1.10×10^{-3}
Propanol	1	1167	1516	1.51190	31.9	2.70×10^{-1}	1.12×10^{1}	3.30×10^{-3}

Table S8. Group-based average of (A) physicochemical parameters, and (B) simulation-derived parameters. Error reported as standard error (±SEM). The following parameters are displayed: number (#) of h-bond donor, number (#) of h-bond acceptor ($H_{acceptor}$), octanol-water coefficient (Log *P*), molecular weight (MW; g), dipole moment (DP; Debye), polar surface area (Å^2), bilayer-drug residence time ($t_{residence}$; ns), number of failed transitions per simulation time (N_{failed}/t_{sim}; ns^{-1}), % of successful transitions, and barriers ΔG_1, ΔG_2, ΔG_3.

Group avg.	H_{donor}	H_{accept}	Log *P*	MW (g)	DP (Debye)	Polar surface area
1	1.9 ± 0.8	3.9 ± 1	0.0 ± 0.4	181.6 ± 64	3.8 ± 1	74.0 ± 20
2	1.5 ± 0.4	3.5 ± 0.4	2.1 ± 0.4	295.4 ± 30	3.9 ± 0.5	57.8 ± 6
3	1.2 ± 0.2	2.7 ± 0.4	3.7 ± 0.4	259.9 ± 20	2.4 ± 0.4	33.2 ± 5
Group avg.	Bilayer-drug $t_{residence}$ (ns)	N_{failed}/t_{sim} (ns^{-1})	% transition	ΔG_1 (kcal mol^{-1})	ΔG_2 (kcal mol^{-1})	ΔG_3 (kcal mol^{-1})
1	8.55 ± 0.2	214 ± 56	0.1 ± 0.1	0.0 ± 0.2	6.0 ± 0.7	6.0 ± 0.7
2	5.94 ± 0.3	27 ± 13	2.2 ± 0.7	-1.2 ± 0.2	5.7 ± 0.6	5.7 ± 0.2
3	4.23 ± 0.7	3.3 ± 1	4.2 ± 0.7	-1.3 ± 0.6	5.6 ± 0.4	5.6 ± 0.6

References

1. Lundborg, M.; Wennberg, C. L.; Narangifard, A.; Lindahl, E.; Norlén, L., Predicting drug permeability through skin using molecular dynamics simulation. *J. Controlled Release* **2018,** *283*, 269-279.
2. Venable, R. M.; Krämer, A.; Pastor, R. W., Molecular dynamics simulations of membrane permeability. *Chem. Rev.* **2019,** *119* (9), 5954-5997.
3. Badaoui, M.; Kells, A.; Molteni, C.; Dickson, C. J.; Hornak, V.; Rosta, E., Calculating Kinetic Rates and Membrane Permeability from Biased Simulations. *The Journal of Physical Chemistry B* **2018,** *122* (49), 11571-11578.
4. Lee, C. T.; Comer, J.; Herndon, C.; Leung, N.; Pavlova, A.; Swift, R. V.; Tung, C.; Rowley, C. N.; Amaro, R. E.; Chipot, C., Simulation-based approaches for determining membrane permeability of small compounds. *J. Chem. Inf. Mod.* **2016,** *56* (4), 721-733.
5. Lindqvist, A.; Fridén, M.; Hammarlund-Udenaes, M., Pharmacokinetic considerations of nanodelivery to the brain: Using modeling and simulations to predict the outcome of liposomal formulations. *Eur. J. Pharm. Sci.* **2016,** *92*, 173-182.
6. Shamloo, A.; Pedram, M. Z.; Heidari, H.; Alasty, A., Computing the blood brain barrier (BBB) diffusion coefficient: A molecular dynamics approach. *J. Magn. Magn. Mater.* **2016,** *410*, 187-197.
7. Bennion, B. J.; Be, N. A.; McNerney, M. W.; Lao, V.; Carlson, E. M.; Valdez, C. A.; Malfatti, M. A.; Enright, H. A.; Nguyen, T. H.; Lightstone, F. C., Predicting a drug's membrane permeability: a computational model validated with in vitro permeability assay data. *The Journal of Physical Chemistry B* **2017,** *121* (20), 5228-5237.
8. Brocke, S. A.; Degen, A.; MacKerell Jr, A. D.; Dutagaci, B.; Feig, M., Prediction of Membrane Permeation of Drug Molecules by Combining an Implicit Membrane Model with Machine Learning. *J. Chem. Inf. Mod.* **2018**.
9. Menichetti, R.; Kanekal, K. H.; Bereau, T., Drug–Membrane Permeability across Chemical Space. *ACS Cent. Sci.* **2018**.
10. Dickson, C. J.; Hornak, V.; Bednarczyk, D.; Duca, J. S., Using membrane partitioning simulations to predict permeability of forty-nine drug-like molecules. *J. Chem. Inf. Mod.* **2018,** *59* (1), 236-244.
11. Dror, R. O.; Pan, A. C.; Arlow, D. H.; Borhani, D. W.; Maragakis, P.; Shan, Y.; Xu, H.; Shaw, D. E., Pathway and mechanism of drug binding to G-protein-coupled receptors. *Proc. Natl. Acad. Sci.* **2011,** *108* (32), 13118-13123.
12. Wise, J. G., Catalytic transitions in the human MDR1 P-glycoprotein drug binding sites. *Biochem.* **2012,** *51* (25), 5125-5141.
13. Khandelwal, A.; Lukacova, V.; Comez, D.; Kroll, D. M.; Raha, S.; Balaz, S., A combination of docking, QM/MM methods, and MD simulation for binding affinity estimation of metalloprotein ligands. *Journal of medicinal chemistry* **2005,** *48* (17), 5437-5447.
14. De Vivo, M.; Masetti, M.; Bottegoni, G.; Cavalli, A., Role of molecular dynamics and related methods in drug discovery. *Journal of medicinal chemistry* **2016,** *59* (9), 4035-4061.
15. Feng, M., Assessment of blood-brain barrier penetration: in silico, in vitro and in vivo. *Current drug metabolism* **2002,** *3* (6), 647-657.
16. Garg, P.; Verma, J., In silico prediction of blood brain barrier permeability: an artificial neural network model. *Journal of chemical information and modeling* **2006,** *46* (1), 289-297.

17. Mensch, J.; Oyarzabal, J.; Mackie, C.; Augustijns, P., In vivo, in vitro and in silico methods for small molecule transfer across the BBB. *Journal of pharmaceutical sciences* **2009,** *98* (12), 4429-4468.
18. Liu, X.; Tu, M.; Kelly, R. S.; Chen, C.; Smith, B. J., Development of a computational approach to predict blood-brain barrier permeability. *Drug metabolism and disposition* **2004,** *32* (1), 132-139.
19. Carpenter, T. S.; Kirshner, D. A.; Lau, E. Y.; Wong, S. E.; Nilmeier, J. P.; Lightstone, F. C., A method to predict blood-brain barrier permeability of drug-like compounds using molecular dynamics simulations. *Biophysical journal* **2014,** *107* (3), 630-641.
20. Wang, Y.; Gallagher, E.; Jorgensen, C.; Troendle, E. P.; Hu, D.; Searson, P. C.; Ulmschneider, M. B., An experimentally validated approach to calculate the blood-brain barrier permeability of small molecules. *Scientific reports* **2019,** *9* (1), 6117.
21. Spector, A. A.; Hoak, J. C.; Fry, G. L.; Denning, G. M.; Stoll, L.; Smith, J., Effect of fatty acid modification on prostacyclin production by cultured human endothelial cells. *J. Clin. Investigation* **1980,** *65* (5), 1003-1012.
22. Spector, A. A.; Yorek, M. A., Membrane lipid composition and cellular function. *Journal of lipid research* **1985,** *26* (9), 1015-1035.
23. Bénistant, C.; Dehouck, M.-P.; Fruchart, J.-C.; Cecchelli, R.; Lagarde, M., Fatty acid composition of brain capillary endothelial cells: effect of the coculture with astrocytes. *Journal of lipid research* **1995,** *36* (11), 2311-2319.
24. Tewes, B.; Galla, H.-J., Lipid polarity in brain capillary endothelial cells. *Endothelium* **2001,** *8* (3), 207-220.
25. Leonenko, Z.; Finot, E.; Ma, H.; Dahms, T.; Cramb, D., Investigation of temperature-induced phase transitions in DOPC and DPPC phospholipid bilayers using temperature-controlled scanning force microscopy. *Biophysical journal* **2004,** *86* (6), 3783-3793.
26. Leontyev, I.; Stuchebrukhov, A., Accounting for electronic polarization in non-polarizable force fields. *Phys. Chem. Chem. Phys.* **2011,** *13* (7), 2613-2626.
27. Baker, C. M., Polarizable force fields for molecular dynamics simulations of biomolecules. *Wiley Interdiscip. Rev. Comput. Mol. Sci.* **2015,** *5* (2), 241-254.
28. Lopes, P. E.; Lamoureux, G.; Roux, B.; Mackerell, A. D., Jr., Polarizable empirical force field for aromatic compounds based on the classical drude oscillator. *J. Phys. Chem. B* **2007,** *111* (11), 2873-85.
29. Vorobyov, I. V.; Anisimov, V. M.; MacKerell, A. D., Jr., Polarizable empirical force field for alkanes based on the classical Drude oscillator model. *J. Phys. Chem. B* **2005,** *109* (40), 18988-99.
30. Lemkul, J. A.; Huang, J.; Roux, B.; MacKerell, A. D., Jr., An Empirical Polarizable Force Field Based on the Classical Drude Oscillator Model: Development History and Recent Applications. *Chem. Rev.* **2016,** *116* (9), 4983-5013.
31. Kumar, A.; Yoluk, O.; MacKerell Jr, A. D., FFParam: Standalone package for CHARMM additive and Drude polarizable force field parametrization of small molecules. *J. Comput. Chem.* **2019**.
32. Shi, Y.; Xia, Z.; Zhang, J.; Best, R.; Wu, C.; Ponder, J. W.; Ren, P., Polarizable atomic multipole-based AMOEBA force field for proteins. *J. Chem. Theory Comput.* **2013,** *9* (9), 4046-4063.
33. Shah, M. V.; Audus, K. L.; Borchardt, R. T., The application of bovine brain microvessel endothelial-cell monolayers grown onto polycarbonate membranes in vitro to estimate the

potential permeability of solutes through the blood–brain barrier. *Pharmaceutical research* **1989,** *6* (7), 624-627.
34. Avdeef, A., *Absorption and drug development: solubility, permeability, and charge state*. John Wiley & Sons: 2012.
35. Brahm, J., Permeability of human red cells to a homologous series of aliphatic alcohols. Limitations of the continuous flow-tube method. *J. Gen. Physiol.* **1983,** *81* (2), 283-304.
36. Hellinger, É.; Veszelka, S.; Tóth, A. E.; Walter, F.; Kittel, Á.; Bakk, M. L.; Tihanyi, K.; Háda, V.; Nakagawa, S.; Duy, T. D. H., Comparison of brain capillary endothelial cell-based and epithelial (MDCK-MDR1, Caco-2, and VB-Caco-2) cell-based surrogate blood–brain barrier penetration models. *Eur. J. Pharm. Biopharm* **2012,** *82* (2), 340-351.
37. Summerfield, S. G.; Read, K.; Begley, D. J.; Obradovic, T.; Hidalgo, I. J.; Coggon, S.; Lewis, A. V.; Porter, R. A.; Jeffrey, P., Central nervous system drug disposition: the relationship between in situ brain permeability and brain free fraction. *J. Pharmacol. Exp. Ther.* **2007,** *322* (1), 205-213.
38. Adson, A.; Burton, P. S.; Raub, T. J.; Barsuhn, C. L.; Audus, K. L.; Ho, N. F., Passive diffusion of weak organic electrolytes across Caco-2 cell monolayers: Uncoupling the contributions of hydrodynamic, transcellular, and paracellular barriers. *Journal of pharmaceutical sciences* **1995,** *84* (10), 1197-1204.
39. Yamashita, S.; Furubayashi, T.; Kataoka, M.; Sakane, T.; Sezaki, H.; Tokuda, H., Optimized conditions for prediction of intestinal drug permeability using Caco-2 cells. *Eur. J. Pharm. Sci.* **2000,** *10* (3), 195-204.
40. Zhang, C.; Chanteux, H.; Zuo, Z.; Kwan, P.; Baum, L., Potential role for human P-glycoprotein in the transport of lacosamide. *Epilepsia* **2013,** *54* (7), 1154-1160.
41. Katt, M. E.; Mayo, L. N.; Ellis, S. E.; Mahairaki, V.; Rothstein, J. D.; Cheng, L.; Searson, P. C., The role of mutations associated with familial neurodegenerative disorders on blood–brain barrier function in an iPSC model. *Fluids Barriers CNS* **2019,** *16* (1), 20.
42. Sun, D.; Lennernas, H.; Welage, L. S.; Barnett, J. L.; Landowski, C. P.; Foster, D.; Fleisher, D.; Lee, K.-D.; Amidon, G. L., Comparison of human duodenum and Caco-2 gene expression profiles for 12,000 gene sequences tags and correlation with permeability of 26 drugs. *Pharmaceutical research* **2002,** *19* (10), 1400-1416.
43. Pade, V.; Stavchansky, S., Link between drug absorption solubility and permeability measurements in Caco-2 cells. *Journal of pharmaceutical sciences* **1998,** *87* (12), 1604-1607.
44. Garberg, P.; Ball, M.; Borg, N.; Cecchelli, R.; Fenart, L.; Hurst, R.; Lindmark, T.; Mabondzo, A.; Nilsson, J.; Raub, T., In vitro models for the blood–brain barrier. *Toxicol. In Vitro* **2005,** *19* (3), 299-334.
45. Lockman, P. R.; McAfee, G.; Geldenhuys, W. J.; Van der Schyf, C. J.; Abbruscato, T. J.; Allen, D. D., Brain uptake kinetics of nicotine and cotinine after chronic nicotine exposure. *J. Pharmacol. Exp. Ther.* **2005,** *314* (2), 636-642.
46. Di, L.; Kerns, E. H.; Bezar, I. F.; Petusky, S. L.; Huang, Y., Comparison of blood–brain barrier permeability assays: in situ brain perfusion, MDR1-MDCKII and PAMPA-BBB. *Journal of pharmaceutical sciences* **2009,** *98* (6), 1980-1991.
47. Yang, X.; Duan, J.; Fisher, J., Application of physiologically based absorption modeling to characterize the pharmacokinetic profiles of oral extended release methylphenidate products in adults. *PloS one* **2016,** *11* (10), e0164641.